Nonautonomous matter waves in a waveguide

Zhenya Yan,[1] Xiao-Fei Zhang,[2,3] and W. M. Liu[2]

[1]*Key Laboratory of Mathematics Mechanization, Institute of Systems Science, AMSS, Chinese Academy of Sciences, Beijing 100190, China*

[2]*Beijing National Laboratory for Condensed Matter Physics, Institute of Physics, Chinese Academy of Sciences, Beijing 100190, China*

[3]*College of Science, Honghe University, Mengzi 661100, China*

(Received 25 October 2010; revised manuscript received 4 July 2011; published 19 August 2011)

We present a physical model that describes the transport of Bose-Einstein-condensed atoms from a reservoir to a waveguide. By using the similarity and Möbius transformations, we study nonautonomous matter waves in Bose-Einstein condensates in the presence of an inhomogeneous source. Then, we find its various types of exact nonautonomous matter-wave solutions, including the W-shaped bright solitary waves, W-shaped and U-shaped dark solitary waves, periodic wave solutions, and rational solitary waves. The results show that these different types of matter-wave structures can be generated and effectively controlled by modulating the amplitude of the source. Our results may raise the possibility of some experiments and potential applications related to Bose-Einstein condensates in the presence of an inhomogeneous source.

DOI: 10.1103/PhysRevA.84.023627 PACS number(s): 03.75.Lm, 03.75.Kk, 05.45.Yv

I. INTRODUCTION

The nonlinear Schrödinger (NLS) equation has extensively drawn much attention due to its numerous physical applications in many branches of nonlinear science, such as nonlinear fiber optics [1–3] and Bose-Einstein condensates (BECs) [4–7] in which the NLS equation is also known as the Gross-Pitaevskii (GP) equation. The standard NLS equation is completely integrable [8] and possesses many types of solitons (e.g., bright solitons, dark solitons, gray solitons, multisoliton solutions, etc.) [9–12]; however, the quasi-one-dimensional or higher-dimensional NLS or GP equations with space- and/or time-modulated coefficients [4–6] may generate nonlinear physical phenomena, such as nonautonomous solitons [13–15], resonant solitons, and breathing solitons [16,17], vortex solitons [18–21], vector solitons [22], and ring dark solitons [23] by modulating external potentials and nonlinearities as well as gain or loss terms. They are in general nonintegrable and difficultly solved. Recently, symmetry analysis provides a powerful way to exactly investigate nonautonomous solutions (also called self-similar solutions) of nonlinear physical models [12–17,24–27], which means that the wave profiles remain unchanged and their amplitudes and widths simply scale with time or propagation distance [13].

It should be pointed out that the above-mentioned works in nonlinear optics have been mainly focused on the study of exact self-similar wave propagation in single-core fibers. In fact, the twin-core fibers, which originate from the linear coupling between thee two fibers, can easily be fabricated [28–30]. Very recently, some attention has also been paid to the study of exact nonlinear waves in twin-core fibers, such as the NLS equation with a source [31], the generalized NLS equation with a source [32], and the higher-order NLS equation with a source [33].

Moreover, the quasi-one-dimensional (1D) time-dependent GP equation in the presence of an inhomogeneous source $S_0 \exp(-i\mu t/\hbar)\delta(x - x_0)$, which models the coupling of a reservoir of Bose-Einstein-condensed atoms to the waveguide, has also attracted much attention [34]. The source term is located at a position $x = x_0$ in the upstream region and emitting monochromatic matter waves, and simulates the coupling of a reservoir of Bose-condensed matters to the waveguide at a given chemical potential, from which matter waves are injected into the waveguide [34–39]. Furthermore, the two-dimensional case [38] and the coupled case [39] in the presence of source terms have also been considered. In addition, the coupling drive (it in fact plays the role of an inhomogeneous source) has been used to transfer phase-sensitive population between two condensates $|F = 1, m_f = -1\rangle$ and $|F = 2, m_F = 1\rangle$. The above-mentioned coupling drive admits an effective frequency of 6834.6774 MHz and is detuned slightly ($\sim$100 Hz) from the expected transition frequency in our trap [40].

In this paper, we consider a model that simulates the coupling of a reservoir of Bose-Einstein-condensed atoms and the waveguide, as shown in Fig. 1. Condensate at a given chemical potential is injected into the waveguide from a reservoir at x_0. The reservoir emits a plane matter wave in both directions into the guide. Here, we go beyond previous studies by considering the case with time- and space-modulated potential and inhomogeneous source, as well as time-modulated nonlinearity and gain or loss terms in BECs, which is in the form of

$$i\hbar\frac{\partial\psi}{\partial t} = \left[-\frac{\hbar^2}{2m}\frac{\partial^2}{\partial x^2} + V_{\rm ext}(x,t) + g_{\rm 1D}(t)|\psi|^2 + i\Gamma(t)\right]\psi + S(t)\exp[i\varphi(x,t)], \quad (1)$$

where $\psi \equiv \psi(x,t)$ is the macroscopic wave function of the condensate, m is the mass of atom, the nonlinearity $g_{\rm 1D}(t) = 2\hbar\omega_\perp a_s(t)$ is the effective 1D coupling strength with $\omega_\perp$ being the transverse confining frequency and $a_s(t)$ being the time-dependent s-wave scattering length modulated by a Feshbach resonance ($a_s(t) > 0$ for a repulsive interaction and $a_s(t) < 0$ for an attractive interaction). $V_{\rm ext}(x,t)$ denotes the time- and space-modulated external potential and can be chosen as the second-degree polynomial in space with all coefficients being functions of time. $\Gamma(t)$ stands for the time-dependent gain or loss distribution. Finally, $S(t)\exp[i\varphi(x,t)]$, with the time-dependent amplitude $S(t)$ and phase $\varphi(x,t)$, simulates the coherent injection of matter waves from an external reservoir onto the scattering region [34,35,38]. It should be pointed out that the losses are caused by the collisions between thermal

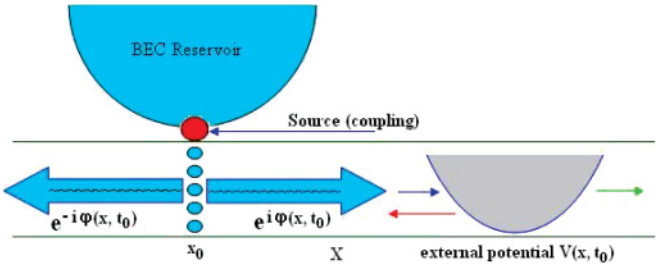

FIG. 1. (Color online) Schematics of the coupling of a reservoir of Bose-Einstein-condensed atoms and the waveguide. Condensate at a given chemical potential is injected into the waveguide from a reservoir at x_0. The reservoir emits a plane matter wave in both directions into the guide. Shown in the right part is the external potential added along the axis direction of the waveguide.

atoms, which is a three-body physical course. Otherwise, the system should be described in a different way (such as a two-degenerate system with a coupling term) [41]. Furthermore, by making the ideal assumption, we neglect the heating effects, which will indeed heat the atoms remaining in the waveguide and play a role for the parameters of the propagation of the matter wave.

Normalizing the length and time in Eq. (1) by $a_\perp = \sqrt{\hbar/(m\omega_\perp)}$ and $\omega_\perp^{-1}$, we arrive at an effective GP equation with an inhomogeneous source term in the dimensionless form

$$i\frac{\partial\psi}{\partial t} = \left[-\frac{1}{2}\frac{\partial^2}{\partial x^2} + v(x,t) + g(t)|\psi|^2 + i\gamma(t)\right]\psi + s(t)\exp[i\varphi(x,t)], \tag{2}$$

where the external potential $v(x,t)$, the nonlinearity $g(t)$, the gain or loss distribution $\gamma(t)$ and the source $s(t)\exp[i\varphi(x,t)]$ are related to the external potential $V_{\rm ext}(x,t)$, nonlinearity $g_{\rm 1D}(t)$, the gain or loss term $\Gamma(t)$, and the source term $S(t)\exp[i\varphi(x,t)]$ in Eq. (1), respectively. Equation (2) is associated with $\delta\mathcal{L}/\delta\psi^\dagger = 0$ in which the Lagrangian density can be written as $\mathcal{L} = i(\psi\psi_t^\dagger - \psi_t\psi^\dagger) + |\psi_x|^2 + 2[v(x,t) + i\gamma(t)]|\psi|^2 + g(t)|\psi|^4 + 2s(t)\exp[i\varphi(x,t)]\psi^\dagger$, where $\psi^\dagger(x,t)$ denotes the complex conjugate of the wave function $\psi(x,t)$.

To translate our results into units relevant to the experiments [34], in this paper, our calculations are performed for ^{87}Rb atoms with $m = 1.44\times10^{-25}$ Kg, $\omega_\perp = 2\pi\times10^3$ s^{-1} for repulsive interaction. In this case, a unity of the dimensionless space corresponds to $a_\perp = \sqrt{\hbar/(m\omega_\perp)} \simeq 0.34$ μm, and a unity of the dimensionless time corresponds to 1.6×10^{-4} s. For the attractive case, we focus on ^{7}Li atoms with $m = 1.17\times10^{-26}$ Kg, and a unity of the dimensionless space corresponds to $a_\perp = \sqrt{\hbar/(m\omega_\perp)} \simeq 1.19$ μm. Here, we want to point out that in the following discussion, both the space and time extent of the obtained solutions are all in the range of quasi-one-dimensional validity. Furthermore, we focus on various nonautonomous matter waves of Eq. (2), which generate new matter-wave structures (e.g., W-shaped bright matter waves and U-shaped dark matter waves illustrated in Sec. III) and can be controlled by the modulation of the inhomogeneous source.

The rest of the paper is organized as follows. In Sec. II, by using the similarity transformation, the 1D time-dependent GP equation in the presence of an inhomogeneous source term (2) is reduced to the stationary GP equation with a constant source. In Sec. III, the distinguished types of Möbius transformations [33] are employed to the stationary GP equation with a constant source. We find various types of exact nonautonomous solutions of Eq. (2), such as rational wave solutions, W-shaped bright solitary wave solutions, periodic wave solutions, and W-shaped and U-shaped dark solitary wave solutions, by modulating the source amplitude. Moreover, we discuss the effects of both the inhomogeneous source and gain or loss amplitudes on the propagation of matter waves. Finally, Sec. IV presents the conclusions of this study.

II. THE TRANSFORMATIONS AND CONSTRAINTS

A. The transformations

We here focus on spatially localized and temporally manipulated nonautonomous solutions of Eq. (2). To investigate its exact nonautonomous solutions, we consider the general nonautonomous solutions in the form of [33]

$$\psi(x,t) = \rho(t)e^{i\theta(x,t)}\Phi[\eta(x,t)], \tag{3}$$

connecting solutions of Eq. (2) with those of the stationary GP equation with a constant source

$$\mu\Phi(\eta) = -\frac{d^2\Phi(\eta)}{d\eta^2} + \sigma\Phi^3(\eta) + s_0. \tag{4}$$

Here, the time-dependent function $\rho(t)$ can be used to modulate the amplitude of nonautonomous matter waves, the time- and space-dependent function $\theta(x,t)$ denotes the phase, $\eta(x,t)$ stands for the nonautonomous matter-wave variables, the chemical potential μ, the nonlinear coefficient σ ($\sigma<0$ for the attractive interaction and $\sigma>0$ for the repulsive interaction), and the source amplitude s_0 are all real-valued constants related to the external potential, nonlinearity, and external source in Eq. (2), respectively.

Notice that Eq. (4) in fact differs from the usual stationary NLS equation [i.e., $\mu\Phi(\eta) = -\Phi_{\eta\eta}(\eta) + \sigma\Phi^3(\eta)$] since the source amplitude $s_0 \neq 0$ is required here, which leads Eq. (4) to be nonintegrable. However, the nonzero source amplitude s_0 will play an important role to manipulate many types of localized nonautonomous matter-wave solutions of Eq. (2).

Equation (3) allows us to reduce Eq. (2) to Eq. (4); variables in this reduction can be determined from the requirement for the new field $\Phi(\eta)$ to satisfy Eq. (4). Thus, we substitute transformation (3) into Eq. (2) and, after relatively simple algebra, obtain the following system of partial differential equations:

$$\eta_{xx} = 0, \quad \eta_t + \theta_x\eta_x = 0, \tag{5a}$$

$$2\rho_t + \rho(\theta_{xx} - 2\gamma) = 0, \quad 2s(t) - s_0\rho\eta_x^2 = 0, \tag{5b}$$

$$2g(t)\rho^2 - \sigma\eta_x^2 = 0, \quad 2v(x,t) + \mu\eta_x^2 + \theta_x^2 + 2\theta_t = 0 \tag{5c}$$

under the constraint $\theta(x,t) = \varphi(x,t)$.

B. Constraints for the time- and space-modulated coefficients

Here, we determine these variables in ansatz (3) and coefficients in Eq. (2) by solving the system (5). First, it follows

from Eq. (5a) that we have the self-similar wave variable $\eta(x,t)$ and the phase $\theta(x,t)$ in the form

$$\eta(x,t) = \alpha(t)x + \chi(t), \tag{6}$$

$$\theta(x,t) = \varphi(x,t) = -\frac{\dot{\alpha}(t)}{2\alpha(t)}x^2 - \frac{\dot{\chi}(t)}{\alpha(t)}x + \varphi_0(t), \tag{7}$$

which are similar to the time-dependent GP equation in the absence of an inhomogeneous source [12,25], where the time-dependent function $\alpha(t)$ denotes the inverse of the width of the localized matter waves; the expression $-\chi(t)/\alpha(t)$ stands for the position of its center of mass; and the time-dependent functions $-\dot{\alpha}(t)/[2\alpha(t)]$, $-\dot{\chi}(t)/\alpha(t)$, and $\varphi_0(t)$ in the phase $\varphi(x,t)$ are related to the phase offset, the frequency shift, and the phase-front curvature, respectively.

And then it follows from Eqs. (5b) and (5c) along with Eqs. (6) and (7) that

$$\rho(t) = \rho_0\delta(t)\sqrt{|\alpha(t)|}, \tag{8}$$

$$v(x,t) = v_2(t)x^2 + v_1(t)x + v_0(t), \tag{9}$$

$$s(t) = \frac{1}{2}\rho_0 s_0\delta(t)\alpha^2(t)\sqrt{|\alpha(t)|}, \quad g(t) = \frac{\sigma|\alpha(t)|}{2\rho_0^2\delta^2(t)}, \tag{10}$$

where $\delta(t) = \exp[\int_0^t \gamma(\tau)d\tau]$, ρ_0 is an integration constant and can, without loss of generality, be chosen as $\rho_0 = 1$, the coefficients $v_j(t)\,(j = 1,2,3)$ of the external potential are given by $v_2(t) = \ddot{\alpha}(t)/[2\alpha(t)] - [\dot{\alpha}(t)/\alpha(t)]^2$, $v_1(t) = \ddot{\chi}(t)/\alpha(t) - 2\dot{\chi}(t)\dot{\alpha}(t)/\alpha^2(t)$, and $v_0(t) = -(1/2)[\dot{\chi}(t)/\alpha(t)]^2 - (\mu/2)\alpha^2(t) - \dot{\varphi}_0(t)$ with $\varphi_0(t)$ being an arbitrary differentiable function of time. We may, without loss of generality, choose the phase-front curvature as $\varphi_0(t) \equiv 0$.

It follows from Eqs. (7) and (8) that the gain or loss term $\gamma(t)$ and $\alpha(t)$ (i.e., the inverse of the width of the nonautonomous matter waves) can be used to manipulate the amplitude $\rho(t)$ of the matter-wave solutions, and $\alpha(t)$ and $\chi(t)$ can adjust the the phase offset and the frequency shift of the phase. Moreover, it follows from Eq. (9) that the external potential $v(x,t)$ is a second-degree polynomial in space with their coefficients being functions of time, which just satisfies the condition that the important potential in BECs is chosen as the time-dependent harmonic trapping potential [4–6]. Equation (10) shows that the gain or loss term $\gamma(t)$ can be used to modulate the source amplitude $s(t)$ and nonlinearity $g(t)$. In addition, we find that the two functions $\alpha(t)$ and $\chi(t)$ do affect the amplitude $\rho(t)$, the external potential $v(x,t)$, the phase $\phi(x,t)$, nonlinearity $g(t)$, and the source amplitude $s(t)$. Thus, the abundant matter-wave structures can be generated, which will be investigated in detail for the attractive BECs ($\sigma < 0$) and repulsive BECs ($\sigma > 0$) in Sec. III.

Therefore, we have established a "bridge" (transformation) (3) connecting the solutions of the 1D time-dependent GP equation with an inhomogeneous source term (2) with the well-known solutions of the stationary GP equation with a constant source (4), which can be generated by using the Möbius transformations [31,33]

$$\Phi(\eta) = \frac{a + b\,\phi^j(\eta)}{1 + c\,\phi^j(\eta)} \quad (j = 1,2) \tag{11}$$

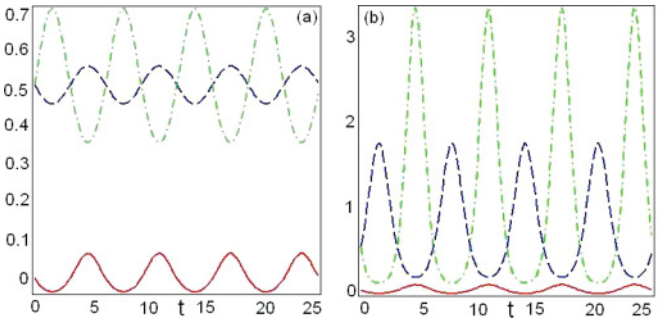

FIG. 2. (Color online) Profiles of the coefficient $v_2(t)$ (solid line) of second-degree term of the linear potential $v(x,t)$ given by Eq. (9), nonlinearity $g(t)$ (dashed line), and the source term $s(t)$ (dashed-dotted line) given by Eq. (10). The parameters are defined by Eq. (12) with $\sigma = \rho_0 = s_0 = 1$. (a) $\gamma_0 = 0.1$, (b) $\gamma_0 = 1$.

connecting solutions of Eq. (4) with those of the stationary NLS equation $\phi_{\eta\eta}(\eta) = c_1\phi(\eta) + c_2\phi^3(\eta)$ with a, b, c and $c_{1,2}$ being all real-valued constants.

C. Choice of the parameters

To make sure that the amplitude $\rho(t)$ and nonlinearity $g(t)$ are bounded for realistic cases, we choose $\alpha(t)$, $\chi(t)$, and $\gamma(t)$ as the localized periodic functions in the form

$$\begin{aligned} \alpha(t) &= 1 + 0.1\sin(t), \\ \chi(t) &= 2 + \cos(t), \\ \gamma(t) &= \gamma_0\cos(t), \end{aligned} \tag{12}$$

where γ_0 is called the gain or loss amplitude that can be used to control different types of matter-wave structures.

Figure 2 displays the profiles of the coefficient $v_2(t)$ of second-degree terms of the external potential $v(x,t)$ given by Eq. (9), nonlinearity $g(t)$, and the inhomogeneous source amplitude $s(t)$ given by Eq. (10) for the chosen parameters given by Eq. (12).

In the following, we will investigate many types of nonautonomous matter-wave solutions of Eq. (2) for the attractive ($\sigma < 0$) and repulsive ($\sigma > 0$) nonlinearities by means of similarity transformation (3) and solutions of the stationary GP equation with a constant source (4) obtained by means of the Möbius transformation (11).

III. NONAUTONOMOUS MATTER-WAVE SOLUTIONS

A. The attractive nonlinearity $\sigma = -1$

1. The rational solution

We here consider the Möbius transformation with the rational form $\Phi(\eta) = (a + b\eta^2)/(1 + c\eta^2)$, which is in fact a modification of the transformation $\Phi(\eta) = [a\phi^2(\eta) + b]/[\phi^2(\eta) + c]$ with $\phi(\eta) = 1/\eta$ being a rational solution of the elliptic equation $\phi_{\eta\eta}(\eta) = c_1\phi(\eta) + c_2\phi^3(\eta)$ (here $c_1 = 0$ and $c_2 = 2$) [33]. After some algebra, we obtain the rational bright solitary wave solutions of Eq. (2).

Case I (*Rational formal bright soliton solutions*):

$$\psi_{\rm rs}(x,t) = \rho(t)e^{i\theta(x,t)}\frac{3\sqrt[3]{4s_0} - 2s_0\,\eta^2}{2\left(1 + \sqrt[3]{2s_0^2}\,\eta^2\right)}, \tag{13}$$

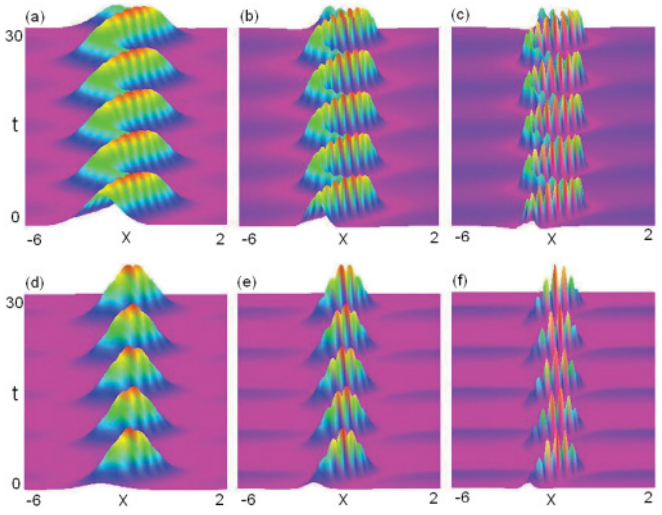

FIG. 3. (Color online) Wave propagations for the intensity distribution $|\psi_{rs}|^2$ given by Eq. (13). (a) $\gamma_0 = 0.1$, $s_0 = 0.2$, (b) $\gamma_0 = 0.1$, $s_0 = 2$, (c) $\gamma_0 = 0.1$, $s_0 = 20$, (d) $\gamma_0 = 1$, $s_0 = 0.2$, (e) $\gamma_0 = 1$, $s_0 = 2$, (f) $\gamma_0 = 1$, $s_0 = 20$.

where the negative chemical potential is given by $\mu = -3/2\sqrt[3]{2s_0^2}$, η, $\theta(x,t)$, and $\rho(t)$ are given by Eqs. (6)–(8), respectively. In particular, $|\psi_{rs}(x,t)| \to 2|s_0|/\sqrt[3]{2s_0^2}\,|\rho(t)|$ as $x \to \infty$.

Figure 3 illustrates the intensity distribution of the localized rational solutions (13) for different source amplitude s_0 and gain or loss amplitude γ_0. As shown in this figure, when the gain or loss amplitude γ_0 becomes large (e.g., $\gamma_0 = 1$), the amplitude of the solitons close to the corners attenuates rapidly so that the soliton chain are generated [see Figs. 3(d)–3(f)].

Moreover, for a fixed gain or loss amplitude γ_0 (e.g., $\gamma_0 = 0.1$ or 1), the strong quasiperiodic oscillations in matter-wave structures are generated and the widths of the solutions decrease with the source amplitude s_0 [see top or bottom (from left to right, i.e., $s_0 = 0.2, 2, 20$) of Fig. 3].

2. *The periodic cn²-wave solution*

If we employ the Möbius transformation with the elliptic function in the form of $\Phi(\eta) = [a + b\,\mathrm{cn}^2(\eta,k)]/[1 + c\,\mathrm{cn}^2(\eta,k)]$ with the modulus $k \in [0, 1]$, and then insert the ansatz into Eq. (4). We can obtain the following solutions for the different modulus k. For example, we choose the modulus as $k = 1, 0, 0.5$ corresponding to the bright solitary waves, trigonometric function solutions, and periodic cn^2-wave solutions, respectively.

Case II (*Bright soliton solutions for* $k = 1$):

$$\psi_{\mathrm{bs}}(x,t) = \rho(t)e^{i\theta(x,t)}\frac{(2c+1) - c(2c+3)\,\mathrm{sech}^2\eta}{\sqrt{-2c(c+1)}(1 + c\,\mathrm{sech}^2\eta)}. \qquad (14)$$

Here, η, $\theta(x,t)$, and $\rho(t)$ are given by Eqs. (6)–(8), respectively. We introduce the parameter c with the condition $-1 < c < 0$ and $c \neq -0.5$ to simply the expression of the solutions (14) [42], which is in fact related to the source amplitude $s_0 = (2c+1)/[c(c+1)\sqrt{-2c(c+1)}]$ and the chemical potential $\mu = (4c^2 + 4c + 3)/[2c(c+1)]$. Thus, we can in principle replace the parameter c with the source amplitude s_0 and the chemical potential μ by solving the equation $s_0 = (2c+1)/[c(c+1)\sqrt{-2c(c+1)}]$. Note that we have $|\psi_{\mathrm{bs}}(x,t)| \to |(2c+1)\rho(t)|/\sqrt{-2c(c+1)} \neq 0$ as $x \to \infty$, since $s_0 \neq 0$ (i.e., $c \neq -0.5$) is required here.

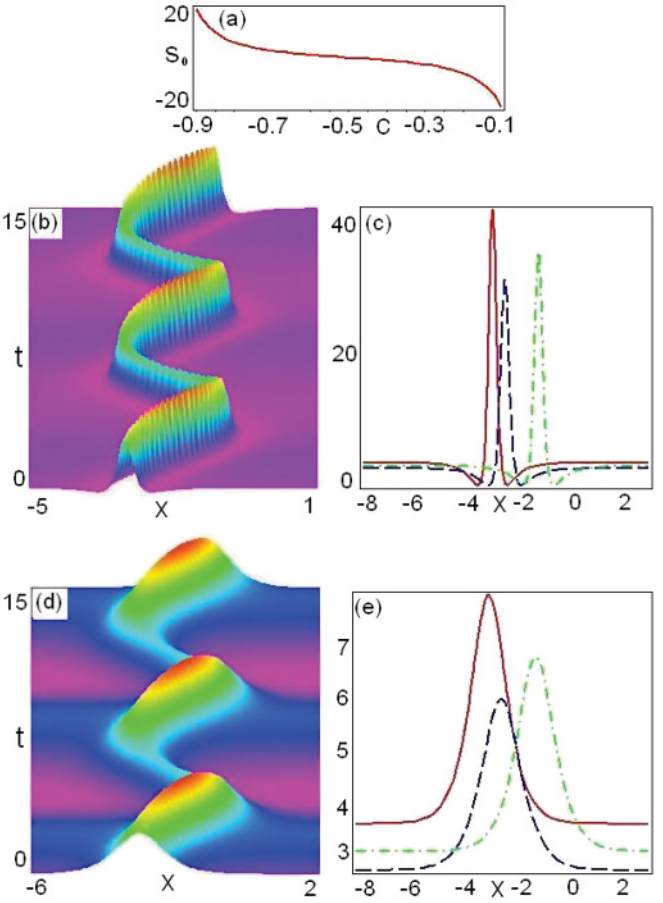

FIG. 4. (Color online) Wave propagations for the intensity distribution $|\psi_{\mathrm{bs}}|^2$ given by Eq. (14) with $\gamma_0 = 0.1$. (a) The source amplitude s_0 vs the parameter c. (b) W-shaped profile with $s_0 = 20.95$ (i.e., $c = -0.9$). (c) The W-shaped profiles vs x with $s_0 = 20.95$ (i.e., $c = -0.9$) and $t = 0$ (solid line), 5 (dashed line), 10 (dashed-dotted line). (d) The bell-shaped profile with $s_0 = -20.95$ (i.e., $c = -0.1$). (e) The bell-shaped profiles vs x with $s_0 = -20.95$ (i.e., $c = -0.1$) and $t = 0$ (solid line), 5 (dashed line), 10 (dashed-dotted line).

The bright solitary wave solution (14) can display different matter-wave structures for different parameters c, which is related to the source amplitude s_0. When the source amplitude $s_0 \to \infty$ corresponding to $c \to -1$ [see Fig. 4(a)], we have the W-shaped bright solitary waves [see Figs. 4(b) and 4(c)] that differ from the usual bright solitary wave solutions; whereas, when the source amplitude $s_0 \to -\infty$ corresponding to $c \to 0$ [see Fig. 4(a)], we get the bell-shaped bright solitary wave solutions [see Figs. 4(d) and 4(e)].

Moreover, we find that, when the source amplitude s_0 becomes smaller (e.g., from $s_0 = 20.95$ to $s_0 = -20.95$ corresponding to $c = -0.9$ to $c = -0.1$), the wave width of the solutions becomes larger [see Figs. 4(b) and 4(d)]. Note that similarly to Case I shown in Figs. 3(d)–3(f), for the large gain or loss amplitude (e.g., $\gamma_0 = 1$), the amplitudes of the bright

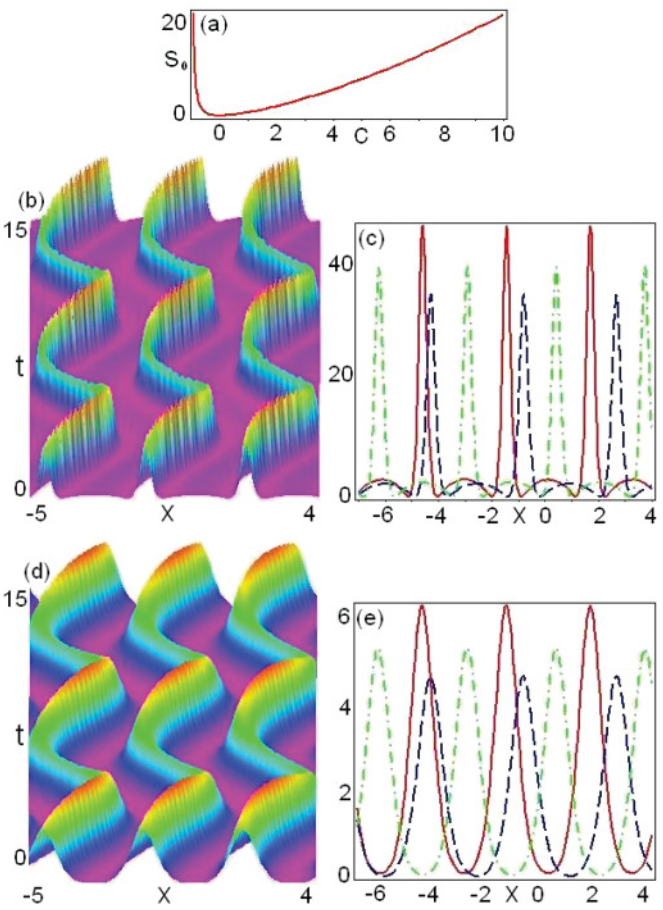

FIG. 5. (Color online) Wave propagations for the intensity distribution $|\psi_{cs}|^2$ given by Eq. (15) with the gain or loss amplitude $\gamma_0 = 0.1$. (a) The source amplitude s_0 vs the parameter c. (b) W-shaped profile with $s_0 = 23.26$ (i.e., $c = 10$). (c) The W-shaped periodic profiles vs x with $s_0 = 23.26$ (i.e., $c = 10$) and $t = 0$ (solid line), 5 (dashed line), 10 (dashed-dotted line). (d) The bell-shaped profile with $s_0 = 0.75$ (i.e., $c = 1$). (e) The bell-shaped periodic profiles vs x with $s_0 = 0.75$ (i.e., $c = 1$) and $t = 0$ (solid line), 5 (dashed line), 10 (dashed-dotted line).

solitary wave solutions (14) close to the corners will almost decrease to zero so that solitary wave chains are generated.

Case III (*Trigonometric function solutions for* $k = 0$):

$$\psi_{cs}(x,t) = \rho(t)e^{i\theta(x,t)}\frac{-(3c+2)+c(c+2)\cos^2\eta}{\sqrt{2(c+1)}(1+c\,\cos^2\eta)}, \qquad (15)$$

where η, $\theta(x,t)$, and $\rho(t)$ are given by Eqs. (6)–(8), respectively, the parameter c is chosen as $c > -1$ with $c \neq 0$ to make sure the solution (15) is localized, $s_0 = c^2(c+2)/[(c+1)\sqrt{2(c+1)}]$, and $\mu = -(3c^2+4c+4)/[2(c+1)]$.

The profiles of the solution (15) are displayed in Figs. 5(b)–5(e). In particular, when the source parameter s_0 becomes large (e.g., $s_0 = 23.26$ corresponding to $c = 10$) [see Fig. 5(a)], resulting in the W-shaped matter waves in one period [see Figs. 5(b) and 5(c)]. Moreover, we find that when the source amplitude s_0 becomes small (e.g., from $s_0 = 22.26$ to 0.75 corresponding to from $c = 10$ to 1), the wave width of the solutions will become large [see Figs. 5(b) and 5(d)].

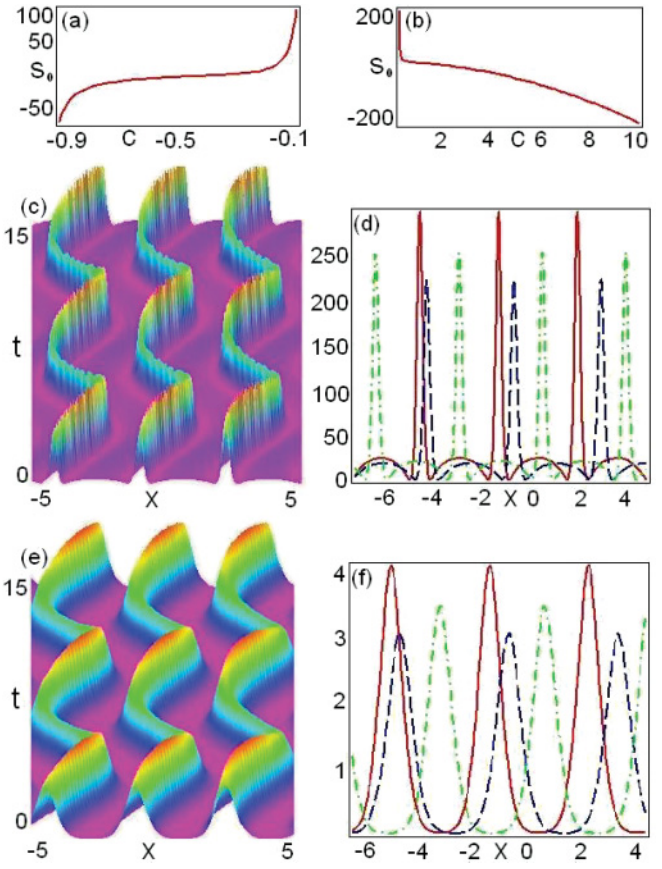

FIG. 6. (Color online) Wave propagations for the intensity distribution $|\psi_{cn}|^2$ given by Eq. (16) with the gain or loss amplitude $\gamma_0 = 0.1$. (a), (b) The source amplitude s_0 vs the parameter c. (c) The W-shaped profile with $s_0 = -926.15$ (i.e., $c = 20$). (d) The W-shaped periodic profiles with $s_0 = -926.15$ (i.e., $c = 20$) and $t = 0$ (solid line), 5 (dashed line), 10 (dashed-dotted line). (e) The bell-shaped profile with $s_0 = -8.72$ (i.e., $c = 2$). (f) The bell-shaped periodic profiles with $s_0 = -8.72$ (i.e., $c = 2$) and $t = 0$ (solid line), 5 (dashed line), 10 (dashed-dotted line).

Case IV (*Periodic* cn^2*-wave solutions for* $k = 0.5$):

$$\psi_{cn}(x,t) = \rho(t)e^{i\theta(x,t)}\frac{a+b\,\mathrm{cn}^2(\eta,k)}{1+c\,\mathrm{cn}^2(\eta,k)}, \qquad (16)$$

where η, $\theta(x,t)$, and $\rho(t)$ are given by Eqs. (6)–(8), respectively, $k = 0.5$, $a = -(9c^2+4c-1)Q/c$, $b = (3c^2+4c-3)Q$, $Q = \sqrt{c/(24c^2+16c-8)}$ with $-1 < c < 0$ and $c > 1/3$, $s_0 = -(27c^6+36c^5-45c^4-15c^2-4c+1)/[4c^2(3c^2+2c-1)]$, and $\mu = -(24c^3+34c^2-8c+3+27c^4)/[8c(3c^2+2c-1)]$.

The profiles of the solution (16) are displayed in Fig. 6. In particular, when the source parameter s_0 becomes small (e.g., $s_0 = -926.15$ corresponding to $c = 20$) [see Fig. 6(a)], it results in the W-shaped matter waves in one period [see Figs. 6(b) and 6(c)].

Moreover, we find that when the source amplitude s_0 becomes small (e.g., from $s_0 = -8.72$ to -925.165 corresponding to from $c = 2$ to 20), the wave width of the solutions will become large [see Figs. 6(b) and 6(d)].

3. The periodic cn-wave solution

Here, we consider the Möbius transformation with the elliptic function in the form of $\Phi(\eta) = [a + b\,\mathrm{cn}(\eta,k)]/[1 + c\,\mathrm{cn}(\eta,k)]$ with the modulus $k \in [0, 1]$. We thus insert the ansatz into Eq. (4) and, after some algebra, obtain the following solutions of Eq. (2) for different modulus k. For example, we choose the modulus $k = 1, 0, 0.8$ corresponding to the bright solitary wave solutions, trigonometric function solutions, and periodic cn-wave solutions, respectively.

Case V (*Bright solitary wave solutions for* $k = 1$):

$$\psi_{\mathrm{bs2}}(x,t) = \rho(t)e^{i\theta(x,t)}\frac{c + (2 - c^2)\,\mathrm{sech}\,\eta}{\sqrt{2(1 - c^2)}(1 + c\,\mathrm{sech}\,\eta)}, \quad (17)$$

where η, $\theta(x,t)$, and $\rho(t)$ are given by Eqs. (6)–(8), respectively, the parameter c is chosen as $-1 < c < 1$ with $c \neq 0$, $s_0 = c/[(c^2 - 1)\sqrt{2(1 - c^2)}]$, and $\mu = (c^2 + 2)/[2(c^2 - 1)]$. The intensity distribution of this solution is similar to the bright solitary wave solutions (14). Note that we have $|\psi_{\mathrm{bs2}}(x,t)| \to 2|\rho(t)|/\sqrt{2(1 - c^2)} \neq 0$ as $x \to \infty$.

The solitary wave solutions exhibit different structures for the parameter c related to the source amplitude s_0 [see Fig. 7(a)]. When the source amplitude $s_0 \to \infty$ corresponding to $c \to -1$ (e.g., $s_0 = 87.94$ corresponding to $c = -0.98$), we have the W-shaped bright solitary wave solution of Eq. (2) [see Figs. 7(b) and 7(c)], which differs from the usual bright solitary wave solutions; whereas, when the source amplitude $s_0 \to -\infty$ corresponding to $c \to 1$ (e.g., $s_0 = 0.83$ corresponding to $c = 0.6$), we have the bell-shaped bright solitary wave solutions of Eq. (2) [see Figs. 7(d) and 7(e)].

Case VI (*Trigonometric function solutions for* $k = 0$):

$$\psi_{\mathrm{cs2}}(x,t) = \rho(t)e^{i\theta(x,t)}\frac{2c^2 - 1 + c\cos\eta}{\sqrt{2(1 - c^2)}(1 + c\,\cos\eta)}, \quad (18)$$

where η, $\theta(x,t)$, and $\rho(t)$ are given by Eqs. (6)–(8), respectively, $-1 < c < 1$ with $c \neq 0$, $s_0 = c^2/[(c^2 - 1)\sqrt{2(1 - c^2)}]$, and $\mu = (2c^2 + 1)/[2(c^2 - 1)]$.

Although the curve change of s_0 versus the parameter c for the solution (18) differs from the one for the solution (15) [see Figs. 8(a) and 5(a)], the intensity distribution of this solution (18) is similar to the trigonometric function solution (15).

Case VII (*Periodic cn-wave solutions for* $k = 0.8$):

$$\psi_{\mathrm{cn2}}(x,t) = \rho(t)\exp[i\theta(x,t)] \times \frac{c(18c^2 + 7) + (32 - 7c^2)\mathrm{cn}(\eta,k)}{Q[1 + c\,\mathrm{cn}(\eta,k)]}, \quad (19)$$

where η, $\theta(x,t)$, and $\rho(t)$ are given by Eqs. (6)–(8), respectively, $k = 0.8$, $Q = \sqrt{800 - 350c^2 - 450c^4}$ with $-1 < c < 1$ and $c \neq 0$, $s_0 = 25c(9c^4 + 16)/[Q(9c^4 + 7c^2 - 16)]$, and $\mu = -(126c^4 - 1777c^2 - 224)/[50(9c^4 + 7c^2 - 16)]$.

Although the curve change of the source amplitude s_0 versus the parameter c for the solution (19) differs from one for the solution (16) [see Figs. 8(b) and 6(a)], the intensity distribution of this solution (19) is similar to the periodic wave solution (16).

4. The periodic dn-wave solution

Here, we consider the Möbius transformation with the elliptic function in the form of $\Phi(\eta) = [a + b\,\mathrm{dn}(\eta,k)]/[1 + c\,\mathrm{dn}(\eta,k)]$ with the modulus $k \in (0, 1]$. We thus insert the ansatz into Eq. (4) and, after some algebra, obtain the following solutions of Eq. (2) for different modulus k. We here choose the modulus as $k = 0.8$ to illustrate the solutions of Eq. (2).

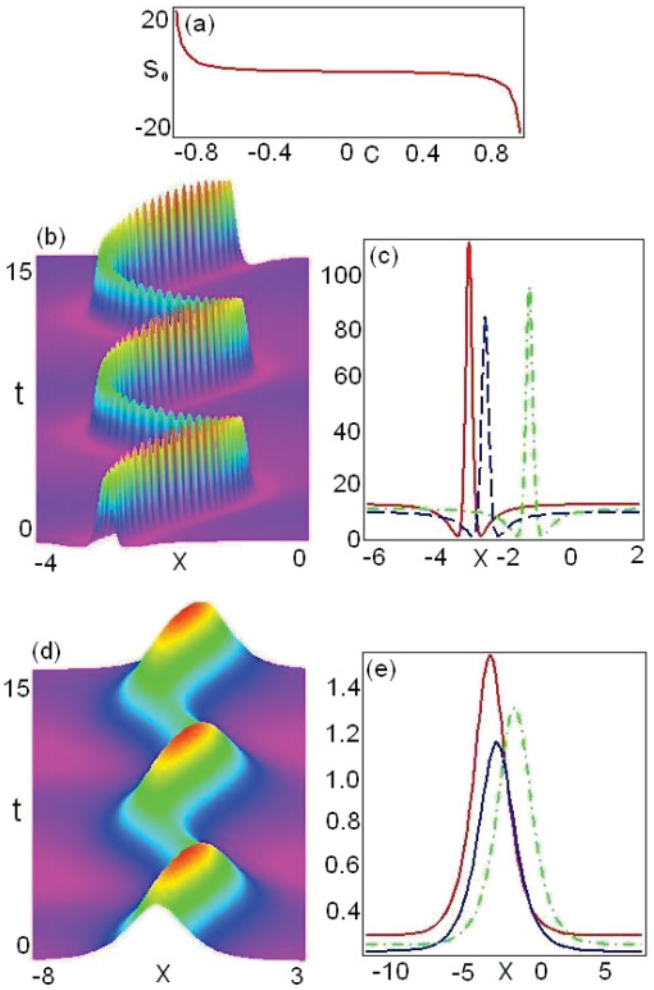

FIG. 7. (Color online) Wave propagations for the intensity distribution $|\psi_{\mathrm{bs2}}|^2$ given by Eq. (17) with the gain or loss amplitude $\gamma_0 = 0.1$. (a) The source amplitude s_0 vs the parameter c. (b) The W-shaped profile with $s_0 = 87.94$ (i.e., $c = -0.98$). (c) W-shaped profiles with $s_0 = 87.94$ (i.e., $c = -0.98$) and $t = 0$ (solid line), 5 (dashed line), 10 (dashed-dotted line). (d) The bell-shaped profile with $s_0 = -0.83$ (i.e., $c = 0.6$). (e) The bell-shaped profiles with $s_0 = -0.83$ (i.e., $c = 0.6$) and $t = 0$ (solid line), 5 (dashed line), 10 (dashed-dotted line).

Case VIII (*Periodic dn-wave solutions with* $k = 0.8$):

$$\psi_{\mathrm{dn}}(x,t) = \rho(t)\exp[i\theta(x,t)] \times \frac{c(9c^2 - 17) + (17c^2 - 25)\mathrm{dn}(\eta,k)}{Q[1 + c\,\mathrm{dn}(\eta,k)]}, \quad (20)$$

where η, $\theta(x,t)$, and $\rho(t)$ are given by Eqs. (6)–(8), respectively, $k = 0.8$, $Q = \sqrt{(225c^4 - 850c^2 + 625)/2}$ with the conditions for the parameter $-5/3 < c < 1$ or $-1 < c < 1$ and $c \neq 0$, or $c > 5/3$, $s_0 = 128c(25 - 9c^4)/[25Q(9c^4 - 34c^2 + 25)]$, and $\mu = -2(153c^4 - 386c^2 + 425)/[25(9c^4 - 34c^2 + 25)]$.

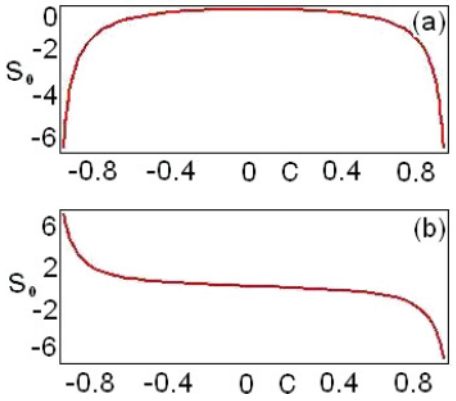

FIG. 8. (Color online) (a) The source amplitude s_0 vs the parameter c for the trigonometric function solution (18). (b) The source amplitude s_0 vs the parameter c for the periodic cn-wave solution (19).

The profiles of the solution (20) are displayed in Fig. 9. There exist three curves for the source s_0 versus the parameter c displayed in Fig. 9. Here, we only consider Fig. 9(b). When the source amplitude s_0 becomes small corresponding to $c \to -1$ (e.g., $s_0 = -11.52$ corresponding to $c = -0.95$) [see Fig. 9(b)], resulting in the W-shaped matter waves in one period [see Figs. 9(d) and 9(e)]. When the source amplitude s_0 becomes large [e.g., $s_0 = -1.35$ corresponding to $c = -0.8$ in Fig. 9(b)], the wave shape is changed into the type of bright soliton solution in one period [see Figs. 9(f) and 9(g)].

B. The repulsive nonlinearity $\sigma = 1$

1. The sech^2-wave solution

For the repulsive nonlinearity $\sigma = 1$, we consider another Möbius transformation with the hyperbolic function in the form $\Phi(\eta) = [a + b\,\mathrm{sech}^2(\eta)]/[1 + c\,\mathrm{sech}^2(\eta)]$. We thus insert the ansatz into Eq. (4) and, after some algebra, obtain the following dark soliton solutions of Eq. (2) in terms of the transformation (3).

Case I (*Dark solitary wave solutions*):

$$\psi_{\mathrm{ds2}}(x,t) = \rho(t)e^{i\theta(x,t)}\frac{-(2c+1)+c(2c+3)\,\mathrm{sech}^2\eta}{\sqrt{2c(c+1)}\,\left(1+c\,\mathrm{sech}^2\eta\right)}, \quad (21)$$

where η, $\theta(x,t)$, and $\rho(t)$ are given by Eqs. (6)–(8), respectively, $c > 0$, $s_0 = -(2c+1)/[c(c+1)\sqrt{2c(c+1)}]$, $\mu = (4c^2+4c+3)/[2c(c+1)]$. Note that we have $|\psi_{\mathrm{ds2}}(x,t)| \to (2c+1)|\rho(t)|/\sqrt{2c(c+1)} \not\equiv 0$ as $x \to \infty$ since $s_0 \neq 0$ (i.e., $c \neq -0.5$) is required here.

Although the form of the soliton (21) is similar to the above-mentioned bright soliton (14), the parameter c is chosen in a different range such that they exhibit different solitary wave structures. Figure 10 displays the profiles of the dark soliton solution (21) for the different source amplitude corresponding to the different parameter c and chemical potential, in which, when the source amplitude s_0 becomes small (e.g., $s_0 = -23.26$ corresponding to $c = 0.1$), the profile becomes the usual dark solitary wave solutions [see Figs. 10(b) and 10(f)]. When the source amplitude s_0 becomes large (e.g., $s_0 = -0.013$ corresponding to $c = 10$), the profile displays the W-shaped dark solitary wave type [see Figs. 10(c) and 10(g)];

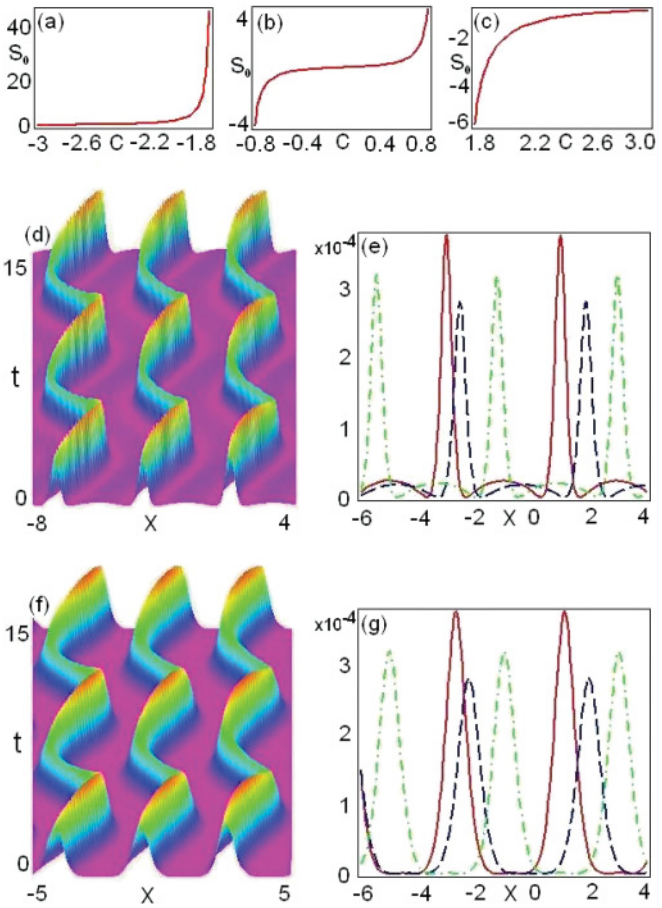

FIG. 9. (Color online) Wave propagations for the intensity distribution $|\psi_{\mathrm{dn}}|^2$ given by Eq. (20) with the gain or loss amplitude $\gamma_0 = 0.1$. (a)–(c) The source amplitude s_0 vs the parameter c. (d) The W-shaped profile with $s_0 = -11.52$ (i.e., $c = -0.95$). (e) W-shaped periodic profiles with $s_0 = -11.52$ (i.e., $c = -0.95$) and $t = 0$ (solid line), 5 (dashed line), 10 (dashed-dotted line). (f) The bell-shaped profile with $s_0 = -1.35$ (i.e., $c = -0.8$). (g) The bell-shaped periodic profiles with $s_0 = -1.35$ (i.e., $c = -0.8$) and $t = 0$ (solid line), 5 (dashed line), 10 (dashed-dotted line).

whereas, when the source amplitude becomes larger (e.g., $s_0 = -3.4 \times 10^{-3}$ corresponding to $c = 20$), the middle part decreases step by step, resulting in the weakly W-shaped dark solitary wave solutions [see Figs. 10(d) and 10(h)]. Finally, as the source amplitude becomes larger (e.g., $s_0 = -8.6 \times 10^{-4}$ corresponding to $c = 40$) again, the middle part will disappear such that the profile of the U-shaped dark solitary wave solutions is found [see Figs. 10(e) and 10(i)]. This implies that the source amplitude s_0 can be used to control the shapes of matter-wave structures.

2. The sech-wave solution

Here, we consider the Möbius transformation with the hyperbolic function in the form of $\Phi(\eta) = [a + b\,\mathrm{sech}(\eta)]/[1 + c\,\mathrm{sech}(\eta)]$. We thus insert the ansatz into Eq. (4) and, after some algebra, obtain the following dark soliton solutions of Eq. (2).

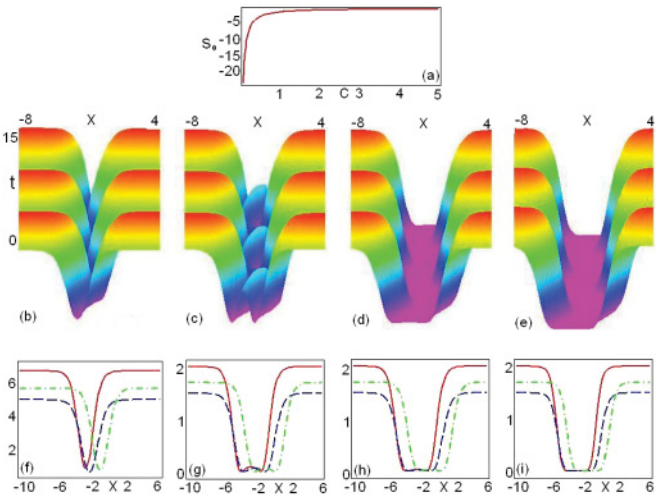

FIG. 10. (Color online) Wave propagations for the intensity distribution $|\psi_{ds2}|^2$ given by Eq. (21) with the gain or loss amplitude $\gamma_0 = 0.1$. (a) The source amplitude s_0 vs the parameter c. (b) The dark solitary waves with $s_0 = -23.26$ (i.e., $c = 0.1$). (c) the W-shaped dark solitary waves with $s_0 = -0.013$ (i.e., $c = 10$). (d) The weak W-shaped dark solitary waves with $s_0 = -3.4 \times 10^{-3}$ (i.e., $c = 20$). (e) The U-shaped dark solitary waves with $s_0 = -8.6 \times 10^{-4}$ (i.e., $c = 40$). (f) The dark solitary waves with $s_0 = 23.25$ (i.e., $c = 0.1$) and $t = 0$ (solid line), 5 (dashed line), 10 (dashed-dotted line). (g) The W-shaped waves with $s_0 = -0.013$ (i.e., $c = 10$) and $t = 0$ (solid line), 5 (dashed line), 10 (dashed-dotted line). (h) The weak W-shaped waves with $s_0 = -3.4 \times 10^{-3}$ (i.e., $c = 20$) and $t = 0$ (solid line), 5 (dashed line), 10 (dashed-dotted line). (i) The U-shaped waves with $s_0 = -8.6 \times 10^{-4}$ (i.e., $c = 40$) and $t = 0$ (solid line), 5 (dashed line), 10 (dashed-dotted line).

Case II (*Dark solitary wave solutions*):

$$\psi_{ds}(x,t) = \rho(t)e^{i\theta(x,t)}\frac{c + (2-c^2)\,\mathrm{sech}\,\eta}{\sqrt{2(c^2-1)}\,(1 + c\,\mathrm{sech}\,\eta)}, \qquad (22)$$

where η, $\theta(x,t)$, and $\rho(t)$ are given by Eqs. (6)–(8), respectively, the parameter c satisfies $c > 1$, and the positive source amplitude and chemical potential are given by $s_0 = c/[(c^2-1)\sqrt{2(c^2-1)}] > 0$ and $\mu = (c^2+2)/[2(c^2-1)] > 0$. Note that we have $|\psi_{ds}(x,t)| \to c|\rho(t)|/\sqrt{2(c^2-1)} \not\equiv 0$ as $x \to \infty$.

Although the form of the soliton (22) is similar to the above-mentioned bright soliton (17), the parameter c is chosen in different ranges such that they exhibit different types of solitary wave solutions. Figure 11 displays the profiles of the dark solitary wave solutions (22) for the parameter c related to the source amplitude and chemical potential. When $s_0 = 0.76$ (i.e., $c = 1.5$), the profile becomes the usual dark solitary wave solutions [see Figs. 11(b) and 11(f)]. As the source amplitude $s_0 \to 0$ (e.g., $s_0 = 7.18 \times 10^{-3}$ corresponding to $c = 10$), the profile displays the W-shaped dark solitary wave solutions [see Figs. 11(c) and 11(g)], whereas the smaller s_0 (e.g., $s_0 = 2.83 \times 10^{-4}$ corresponding to $c = 50$) makes the middle part of the W-shaped dark solitary wave solutions become larger [see Figs. 11(d) and 11(h)]. If we further take smaller source amplitude (e.g., $s_0 = 2.83 \times 10^{-6}$ corresponding to $c = 500$), the middle part of the W-shaped dark solitary wave solutions

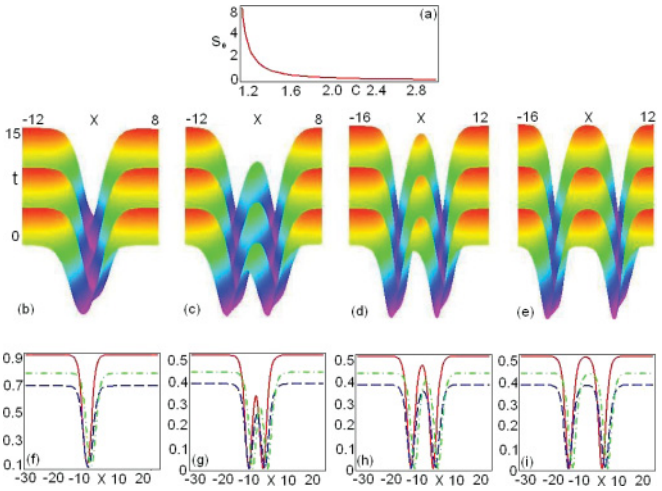

FIG. 11. (Color online) Wave propagations for the intensity distribution $|\psi_{ds}|^2$ given by Eq. (22) with the gain or loss amplitude $\gamma_0 = 0.1$. (a) The source amplitude s_0 vs the parameter c. (b) The dark soliton profile with $s_0 = 0.76$ (i.e., $c = 1.5$). (c)–(e) W-shaped profile with $s_0 = 7.18 \times 10^{-3}$, 2.83×10^{-4}, 2.83×10^{-6} (i.e., $c = 10, 50, 500$). (f) The dark soliton profile with $s_0 = 0.76$ (i.e., $c = 1.5$) and $t = 0$ (solid line), 5 (dashed line), 10 (dashed-dotted line). (g)–(i) The W-shaped profile with $s_0 = 7.18 \times 10^{-3}$, 2.83×10^{-4}, 2.83×10^{-6} (i.e., $c = 10, 50, 500$) and $t = 0$ (solid line), 5 (dashed line), 10 (dashed-dotted line).

becomes larger, but it is less than the amplitudes of both sides [see Figs. 11(e) and 11(i)].

Stability of the solutions against small perturbations, such as thermal noise, is a crucial issue as it is linked with the experimental observation and especially important for gases with repulsive interactions [43]. This can be done by the linear stability theory and numerical simulations of the solutions with perturbations initially implanted. As the object of this paper is to find the exact matter-wave solutions, a thorough analysis of the stability surpasses the scope of this paper and deserves separate studies. We will leave these studies to later publications. Moreover, the technique used in this paper can also be extended to higher-dimensional and/or multicomponent BECs in the presence of inhomogeneous source terms.

IV. CONCLUSIONS

In conclusion, we have studied nonautonomous matter waves in Bose-Einstein condensates in the presence of an inhomogeneous source, and analytically reported many types of exact nonautonomous matter-wave solutions of the 1D time-dependent GP equation in the presence of a source term (2). These obtained nonautonomous matter-wave solutions contain bright solitary waves, dark solitary waves, periodic wave solutions, and rational solitary waves subject to different source amplitudes and gain or loss term. Moreover, the functionalities of the source (s_0) and gain or loss (γ_0) amplitudes are presented to manipulate and control different matter-wave propagation structures. These matter-wave solutions may further raise the possibility of some experiments and potential applications related to BECs in the presence of an inhomogeneous source.

ACKNOWLEDGMENTS

This work was supported by the NSFC under Grants No. 60821002F02, 11071242, 10874235, 10934010, 60978019, and by the NKBRSFC under Grant Nos. 2009CB930701, 2010CB922904, 2011CB302400, and 2011CB921500.

[1] Y. S. Kivshar and G. Agrawal, *Optical Solitons: From Fibers to Photonic Crystals* (Academic, New York, 2003).
[2] C. Sulem and P. Sulem, *The Nonlinear Schrödinger Equation: Self-Focusing and Wave Collapse* (Springer, Berlin, 1999).
[3] B. A. Malomed, D. Mihalache, F. Wise, and L. Torner, J. Opt. B: Quantum Semiclassical Opt. **7**, R53 (2005).
[4] F. Dalfono, S. Giorgini, L. P. Pitaevskii, and S. Stringari, Rev. Mod. Phys. **71**, 463 (1999).
[5] C. J. Pethick and H. Smith, *Bose-Einstein Condensation in Dilute Gases* (Cambridge University Press, Cambridge, 2002).
[6] R. Carretero-González, D. J. Frantzeskakis, and P. G. Kevrekidis, Nonlinearity **21**, R139 (2008).
[7] V. A. Brazhnyi and V. V. Konotop, Mod. Phys. Lett. B **18**, 627 (2004).
[8] C. S. Gardner, J. M. Greene, M. D. Kruskal, and R. M. Miura, Phys. Rev. Lett. **19**, 1095 (1967).
[9] Y. S. Kivshar and B. Luther-Davies, Phys. Rep. **298**, 81 (1998).
[10] Z. X. Liang, Z. D. Zhang, and W. M. Liu, Phys. Rev. Lett. **94**, 050402 (2005).
[11] V. M. Pérez-García, P. Torres, and V. V. Konotop, Phys. D (Amsterdam) **221**, 31 (2006).
[12] Z. Y. Yan and C. Hang, Phys. Rev. A **80**, 063626 (2009).
[13] S. A. Ponomarenko and G. P. Agrawal, Phys. Rev. Lett. **97**, 013901 (2006).
[14] V. N. Serkin and A. Hasegawa, Phys. Rev. Lett. **85**, 4502 (2000).
[15] V. N. Serkin, A. Hasegawa, and T. L. Belyaeva, Phys. Rev. Lett. **98**, 074102 (2007).
[16] J. Belmonte-Beitia, V. M. Pérez-García, V. Vekslerchik, and P. J. Torres, Phys. Rev. Lett. **98**, 064102 (2007).
[17] J. Belmonte-Beitia, V. M. Pérez-García, V. Vekslerchik, and V. V. Konotop, Phys. Rev. Lett. **100**, 164102 (2008).
[18] D. N. Christodoulides *et al.*, Nature (London) **424**, 817 (2003).
[19] N. K. Efremidis, K. Hizanidis, B. A. Malomed, and P. Di Trapani, Phys. Rev. Lett. **98**, 113901 (2007).
[20] J. D. Wang and J. K. Yang, Phys. Rev. A **77**, 033834 (2008).
[21] A. C. Ji, W. M. Liu, J. L. Song, and F. Zhou, Phys. Rev. Lett. **101**, 010402 (2008).
[22] D. S. Hall, M. R. Matthews, J. R. Ensher, C. E. Wieman, and E. A. Cornell, Phys. Rev. Lett. **81**, 1539 (1998); H. Pu and N. P. Bigelow, *ibid.* **80**, 1130 (1998); J. Ieda, T. Miyakawa, and M. Wadati, *ibid.* **93**, 194102 (2004); L. Li, Z. D. Li, B. A. Malomed, D. Mihalache, and W. M. Liu, Phys. Rev. A **72**, 033611 (2005); Z. Y. Yan, K. W. Chow, and B. A. Malomed, Chaos Solitons Fractals **42**, 3013 (2009); X. X. Liu, H. Pu, B. Xiong, W. M. Liu, and J. B. Gong, Phys. Rev. A **79**, 013423 (2009).
[23] Y. S. Kivshar and X. Yang, Phys. Rev. E **50**, R40 (1994); G. Theocharis, D. J. Frantzeskakis, P. G. Kevrekidis, B. A. Malomed, and Y. S. Kivshar, Phys. Rev. Lett. **90**, 120403 (2003).
[24] Z. Y. Yan and V. V. Konotop, Phys. Rev. E **80**, 036607 (2009).
[25] Z. Y. Yan, V. V. Konotop, and N. Akhmediev, Phys. Rev. E **82**, 036610 (2010); Z. Y. Yan, Phys. Lett. A **374**, 672 (2010).
[26] Yu. V. Bludov, Z. Y. Yan, and V. V. Konotop, Phys. Rev. A **81**, 063610 (2010).
[27] V. N. Serkin, A. Hasegawa, and T. L. Belyaeva, Phys. Rev. A **81**, 023610 (2010).
[28] B. A. Malomed, Phys. Rev. E **51**, R864 (1995).
[29] B. A. Malomed, I. M. Skinner, P. L. Chu, and G. D. Peng, Phys. Rev. E **53**, 4084 (1996).
[30] G. Cohen, Phys. Rev. E **61**, 874 (2000).
[31] T. S. Raju, C. Nagaraja Kumar, and P. K. Panigrahi, J. Phys. A: Math. Gen. **38**, L271 (2005).
[32] T. S. Raju, P. K. Panigrahi, and K. Porsezian, Phys. Rev. E **71**, 026608 (2005); **72**, 046612 (2005).
[33] Z. Y. Yan, J. Phys. A: Math. Gen. **39**, L401 (2006).
[34] T. Paul, K. Richter, and P. Schlagheck, Phys. Rev. Lett. **94**, 020404 (2005).
[35] T. Paul, P. Leboeuf, N. Pavloff, K. Richter, and P. Schlagheck, Phys. Rev. A **72**, 063621 (2005).
[36] T. Paul, M. Hartung, K. Richter, and P. Schlagheck, Phys. Rev. A **76**, 063605 (2007).
[37] K. Rapedius and H. J. Korsch, Phys. Rev. A **77**, 063610 (2008).
[38] M. Hartung, T. Wellens, C. A. Müller, K. Richter, and P. Schlagheck, Phys. Rev. Lett. **101**, 020603 (2008).
[39] T. Ernst, T. Paul, and P. Schlagheck, Phys. Rev. A **81**, 013631 (2010).
[40] D. S. Hall, M. R. Matthews, C. E. Wieman, and E. A. Cornell, Phys. Rev. Lett. **81**, 1543 (1998).
[41] N. K. Whitlock and I. Bouchoule, Phys. Rev. A **68**, 053609 (2003).
[42] Hereafter, we have introduced the parameter c in exact nonautonomous matter-wave solutions in order to simplify the expressions of these solutions, which is in fact related to the source amplitude s_0 and the chemical potential μ by some formulas. We can in principle replace the parameter c with the source amplitude s_0 by solving these equations about c and s_0 such that we can also express the chemical potential μ by the source amplitude s_0.
[43] C. Mora and Y. Castin, Phys. Rev. A **67**, 053615 (2003).